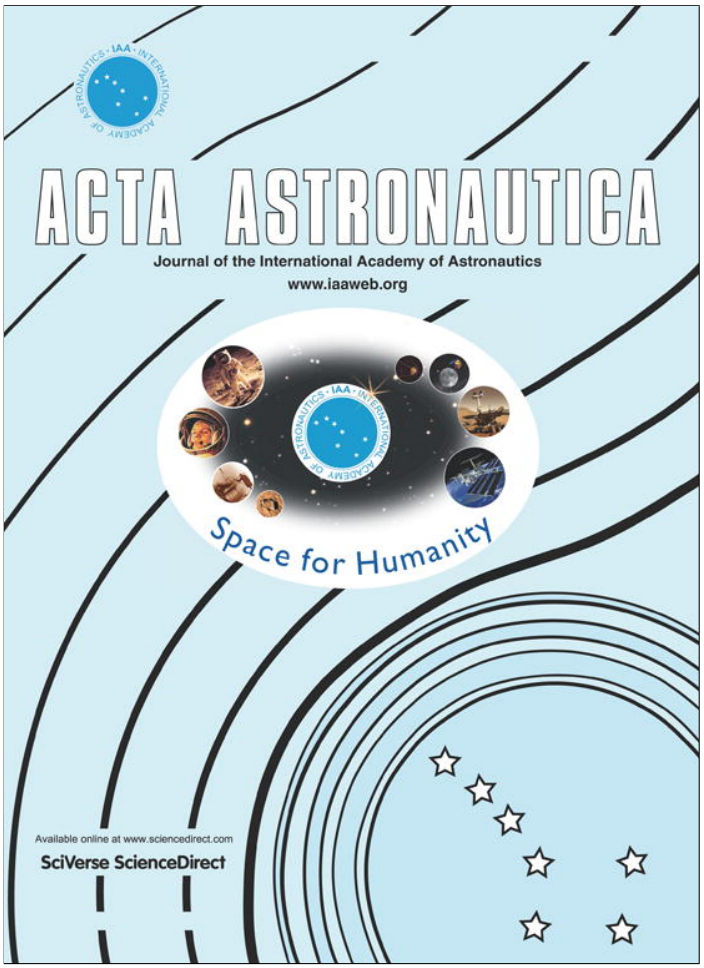

(This is a sample cover image for this issue. The actual cover is not yet available at this time.)

Acta Astronautica 83 (2013) 108–118

Contents lists available at SciVerse ScienceDirect

Acta Astronautica

journal homepage: www.elsevier.com/locate/actaastro

Optimal reconfigurations of two-craft Coulomb formations along manifolds

Drew R. Jones [a,*], Hanspeter Schaub [b]

[a] Aerospace Engineering and Engineering Mechanics Department, WRW Laboratories, The University of Texas at Austin, 210 E 24th Street, Austin, TX 78712, United States

[b] Aerospace Engineering Sciences Department, Colorado Center for Astrodynamics Research, The University of Colorado at Boulder, Boulder, CO 80309, United States

ARTICLE INFO

Article history:
Received 29 May 2012
Received in revised form
5 October 2012
Accepted 18 October 2012

Keywords:
Coulomb formations
Invariant manifolds
Optimal reconfigurations
Particle swarm optimization

ABSTRACT

Coulomb formations refer to swarms of closely flying spacecraft, in which the net electric charge of each vehicle is controlled. Active charge control is central to this concept and enables a propulsion system with highly desirable characteristics, albeit with limited controllability. Numerous Coulomb formation equilibria have been derived, but to maintain and maneuver these configurations, some inertial thrust is required to supplement the nearly propellant-less charge control. In this work, invariant manifold theory is applied to two-craft Coulomb equilibria, which are admitted in a linearized two-body gravity model. The manifolds associated with these systems are analyzed for the first time, and are then utilized as part of a general procedure for formulating optimal reconfigurations. Specifically, uncontrolled flows along the manifolds are sought which provide near continuous transfers from one equilibrium to another. Control is then introduced to match continuity, while minimizing inertial thrusting. This methodology aims to exploit uncontrolled motions and charge control to realize the shape-changing ability of these formations, without large inertial control efforts. Some variations in formulating and parameterizing the optimal transfers are discussed, and analytical expressions are derived to aid in establishing control parameter limits, under certain assumptions. Numerical results are provided, as demonstrative examples of the optimization procedure, using relatively simple control approximations. Finally, Particle Swarm Optimization, a novel stochastic method, is used with considerable success to solve the numerically difficult parameter optimization problems.

1. Introduction

Formations of close-proximity spacecraft have many advantages over a single large craft, including overall mass reduction, shape-changing ability, and multiple launches for deployment, assembly, and repair. Applications for these satellite swarms are many, for example enabling separated space-borne interferometry [1,2]. Initially, electric propulsion (EP) systems were proposed for controlling the relative craft motions; however, EP suffers from limited throttle-ability and introduces the problem of thruster-plume impingement, where thruster ejecta may damage or impede neighboring craft [2]. An alternative to EP for controlling free-flying craft, known as Coulomb thrusting (active charge control), is explored by King et al. in Refs. [2,3]. This concept proposes to servo the electric potential (or net charge) of each vehicle, to yield desired inter-craft forces. The earliest study of active charge control is by John Cover et al. [4], where this mechanism is proposed to inflate and maintain the shape

* Corresponding author.
E-mail address: drjones604@utexas.edu (D.R. Jones).

0094-5765/$ - see front matter © 2012 Elsevier Ltd. All rights reserved.
http://dx.doi.org/10.1016/j.actaastro.2012.10.028

of a large reflecting mesh. This nearly-propellant-less system ($ISP \sim 10^{13}$ s) avoids thruster-plumes, has fast throttling (transition time $\sim$ ms), and can sustain a given force using less power and fuel than EP [2,4]. Proposed applications for this concept include advanced docking/rendezvous, autonomous inspection, contact-less removal of hazardous material, and the deployment/retrieval of instruments [5]. Also, Coulomb thrusting can provide equilibrium forces ($\sim \mu N - mN$) to cancel differential gravity accelerations, resulting in 'virtual structures' or so-called static Coulomb formations. Furthermore, this concept is based on the existing technology, since active control of spacecraft charge was successfully executed during the SCATHA [6] and ATS [7] missions, and currently on the CLUSTER [8] mission. Unfortunately, this propulsion system has a couple of drawbacks. First, Coulomb forces are shielded by the surrounding plasma, which may render charge control infeasible for particular orbit regimes and mission applications. Second, Coulomb thrusting alone provides limited controllability, and cannot alter the overall formation angular momentum [9]. Therefore, it must be supplemented with inertial thrust (e.g. EP or chemical) to enable full controllability, which has led to the adoption of hybrid controllers [10,11].

A wide-variety of static Coulomb formations are derived with respect to a circular reference orbit, analytically for < 5 craft (numerically otherwise), and thus far, all are dynamically unstable [2,5]. Formations with motions referenced to the Hill-frame, a rotating frame with origin at the formation center-of-mass, are considered in the most detail, generally using the linearized Clohessy–Wiltshire–Hill gravitational model [12]. Other known equilibrium include three-craft forms in the absence of gravitational forces [13], two-craft forms in fully non-linear 2-body and circular-restricted 3-body (CRTBP) gravitational models [11], and two- and three-craft spinning configurations [14,15]. Of these spinning configurations, stable 2-body scenarios have been identified where the plasma shielding effect is included in the stability analysis [14]. And a recent study by Hogan and Schaub demonstrates the marginal in-plane stability of particular collinear spinning equilibria if proper separation distance and speed conditions are met [15]. Moreover, the highly nonlinear and coupled system dynamics permit the potential existence of numerous, yet undiscovered, equilibrium and periodic flows (constant or variable potentials).

This research applies invariant manifold theory to two-craft configurations which exist in the two-body gravity Hill-frame model, for the first time. The system manifolds are analyzed, in the interest of exploiting them for station-keeping and maneuvering of the formations. Invariant manifold theory has successfully been used to design low-thrust transfers between regions of space, in multi-body gravity fields, for example in the work of Russell and Lam [16]. Here, manifold theory is applied to Coulomb formations with an analogous purpose. Natural flows along manifolds are sought which 'hop' from unstable to stable branches in order to partially achieve reconfigurations. More generally, it is expected that non-intuitive trajectories and dynamical motions will become more tractable upon applying this theory, which will prove useful in the Coulomb formation design, control, and navigation.

This is a continuation and improvement upon the work of Jones [17], where a generalized procedure for targeting optimal transfers between Coulomb equilibria is outlined. The current method is similar to Jones [17], in that a parameter optimization problem is formulated to differentially correct an uncontrolled, and discontinuous, initial trajectory along manifolds. However, the method details, the dynamical model, and the results have been improved, and applied specifically to two-craft Hill-frame equilibria. Lastly, a unique stochastic method, known as Particle Swarm Optimization (PSO), is used in solving the nonlinear programming problems [18,19].

Much attention is devoted to the development of continuous feedback controllers to maintain Coulomb formations. Controllers are derived and tested by Natarajan and Schaub (in the presence of gravity gradient torque and other disturbances) for the two-craft Hill-frame equilibria [10,20], and by Inampudi for CRTBP equilibrium configurations about Earth–Moon libration points [11]. Some research on realizing the shape-changing ability of these formations is also available. Natarajan [21] presents a feedback control to transfer between the two-craft Hill-frame configurations, and Inampudi adds optimization to that work, by applying a pseudo-spectral discretization method to minimize: time, fuel, and total power usage [11]. Here, optimal reconfigurations between the same equilibria are pursued; however, the problem setup differs substantially, with added emphasis on generality. The current work also contrasts with Inampudi [11], by its utilization of invariant manifold theory and employment of a stochastic rather than a deterministic optimization solver.

2. Coulomb formation background and dynamical model

A conductive surface will naturally exchange ions and electrons with the plasma of space, and as a result will assume a non-zero electric potential ϕ (measured in Volts). In a vacuum, a charged point-mass ϕ varies in proportion to $k_c\, q/r$, where k_c is the Coulomb constant, q the net charge, and r is the radial distance. When immersed in a plasma, this ideal $\phi(r)$ is effectively limited (or shielded) due to interactions with free particles and photons. The Debye length λ_d is used to approximate this shielding, such that a charged particle at a distance $r > \lambda_d$ will not be effected by $\phi(r)$. The λ_d is a measure of the time-dependent local plasma temperature and density, and experimental values for it have been acquired in various regimes (e.g. LEO: 0.02–0.4 m, GEO: 140–1500 m, interplanetary: 7.4–24 m [2]).

Computing ϕ for realistic shapes that interact with a dynamic plasma and with other charged vehicles is somewhat intractable, but can be modeled using the Vlaslov–Poisson partial differential equations. High-fidelity numerical computations of ϕ are available, from finite element analysis techniques and/or experimental data [3,21,22]. Specifically, Stiles et al. [22] discuss that the

potential is bounded above by the vacuum model and below by the conservative Debye–Hückel model (a truncation of the Vlaslov–Poisson). In part, this shows that simple analytical expressions for ϕ (and the resulting electrostatic forces) can be quite accurate under certain conditions. Such conditions are enforced throughout this research, allowing more manageable ϕ models to be used.

A steady-state ϕ occurs when the net current to the vehicle is zero [2], and altering this ϕ artificially has substantial mission heritage [6–8]. This involves utilizing an electron-gun or similar device to eject electrons/ions into the surrounding plasma with sufficient kinetic energy to escape the 'potential-well'. Therefore, the device must have sufficient power P_{out} to supply a voltage equal to the desired ϕ, at a current I_{out} at least greater than the incoming environmental current I_{en} (since this will tend to drive ϕ back towards natural equilibrium).

2.1. General Coulomb formation dynamical model

It is assumed that all spacecraft have a spherical, perfectly conductive, outer surface of uniform charge density of radius R_{sc}, such that all act as equivalent point charges at a distance. These assumptions allow Eq. (1a) to relate ϕ (at R_{sc}) to the net surface charge q, analytically. Also, Eq. (1b) is the result of combining Ohm's law with Eq. (1a), and is an expression for the device power P_{out} and the time required Δt_q to change the potential by a quantity: $|\Delta\phi|$

$$\phi = k_c \frac{q}{R_{sc}} \tag{1a}$$

$$P_{\text{out}} = \phi I_{\text{out}}, \quad \Delta t_q = \frac{|\Delta q|}{I_{\text{out}}} = \frac{R_{sc}|\Delta\phi|}{k_c I_{\text{out}}} \tag{1b}$$

The $\phi_i(t)$ are continuous and controllable functions of time, and can therefore be approximated, to some order, by piecewise polynomial functions. For simplicity, the highest degree polynomial used in this work is the piecewise linear approximation. This contrasts with other studies which maintained $\phi(t)$ as a continuous function, subject to a feedback control law [11,21]. The net Coulomb acceleration of craft i (net charge q_i and mass m_i), denoted $\mathbf{H}_i$, is defined using the Debye–Hückel point-charge model, given by Eqs. (2a) and (2b). This accounts for partial shielding of each potential, using a constant and finite λ_d, where $r_{ij} = \|\mathbf{r}_i - \mathbf{r}_j\|$ is the distance between crafts i and j

$$\mathbf{H}_i = \frac{\mathbf{f}_i}{m_i} = -\frac{R_{sc}^2 \phi_i}{k_c m_i} \sum_{j \neq i} \phi_j \frac{\partial}{\partial \mathbf{r}_i} \left(\frac{e^{-r_{ij}/\lambda_d}}{r_{ij}} \right) \tag{2a}$$

$$\mathbf{H}_i = \frac{\mathbf{f}_i}{m_i} = \frac{R_{sc}^2 \phi_i}{k_c m_i} \sum_{j \neq i} \frac{\phi_j e^{-r_{ij}/\lambda_d}}{r_{ij}^3} \left(1 + \frac{r_{ij}}{\lambda_d} \right) \mathbf{r}_{ij} \tag{2b}$$

It has been demonstrated that this model accurately approximates experimental/numerical solutions for ϕ and $\mathbf{H}_i$, so long as $R_{sc} \ll \lambda_d$ (generally valid at GEO), and $r_{ij} > 10R_{sc}$ [21,22]. Eq. (3) provides the dynamical framework for this work, where in addition to $\mathbf{H}_i$ given by Eq. (2b), terms are included to account for gravitational $\mathbf{G}_i$ and inertial control $\mathbf{u}_i$ accelerations, respectively

$$\ddot{\mathbf{r}}_i = \mathbf{H}_i + \mathbf{G}_i + \mathbf{u}_i \tag{3}$$

In this study, the spacecraft are assumed to be of equal build and type, and holding a similar attitude. Thus, differential solar radiation pressure (SRP) is not considered at this stage. Also, Coulomb force magnitudes being considered here are of at least μN order, and therefore at GEO all perturbing forces, with the exception of SRP, are much smaller, and therefore reasonably neglected in Eq. (3).

In general, any Coulomb formation (of N craft) may be written as a first order ODE system, denoted as $\dot{\mathbf{X}} = \mathbf{F}(\mathbf{X}, \mathbf{X_p}, t)$, where t is the independent variable of integration (assumed time). The state vector $\mathbf{X}$ includes position and velocity vectors ($\mathbf{r}_i$ and $\mathbf{v}_i$), ϕ_i, and possibly mass m_i (if variable), for each craft. The elements of $\mathbf{X_p}$ may be constant or t dependent, and include the control approximating parameters for each $\mathbf{u}_i(t)$ and $\phi_i(t)$. Small state perturbations $\boldsymbol{\delta}\mathbf{X}$ about some reference trajectory $\mathbf{X}^*$, may be considered using the following:

$$\boldsymbol{\delta}\dot{\mathbf{X}} = \left(\frac{\partial \mathbf{F}}{\partial \mathbf{X}} \right) \Big|_{\mathbf{X}^*} \boldsymbol{\delta}\mathbf{X} = \mathbf{A}\boldsymbol{\delta}\mathbf{X} \tag{4}$$

This linearized ODE system for the perturbation vector $\boldsymbol{\delta}\mathbf{X}$, has a Jacobian matrix $\mathbf{A}$ that can be transformed to Jordan canonical form. In this way, the Jacobian matrix may be decomposed into unstable, stable, and center eigenspaces (E^u, E^s, E^c with dimensions N_u, N_s, and N_c, respectively) such that $N = N_u + N_s + N_c$. In this system, perturbations along the E^u basis vectors will grow, whereas those in E^s will dissipate.

2.2. Two-craft Coulomb formation model

The following two-craft model, is a particular case of the general model, and is adopted in this work for the analysis of invariant manifolds and in the optimization of reconfigurations. Both craft's motions are described relative to the Hill-frame, which is centered at and rotates with a nominal center-of-mass (CM) orbit (assumed circular with semi-major-axis a_0 near GEO). The Hill-frame is depicted in Fig. 1, with origin at CM and axes labeled: $\hat{e}_R$ for radial, $\hat{e}_T$ for transverse, and $\hat{e}_N$ for normal. The vehicles then appear statically fixed with respect to the rotating Hill-frame, for equilibrium configurations admitted by this model. The gravitational acceleration of craft 1, is modeled using the linearized Clohessy–Wiltshire–Hill (CW) equations of motion [12], given by Eq. (5a). Then, since the

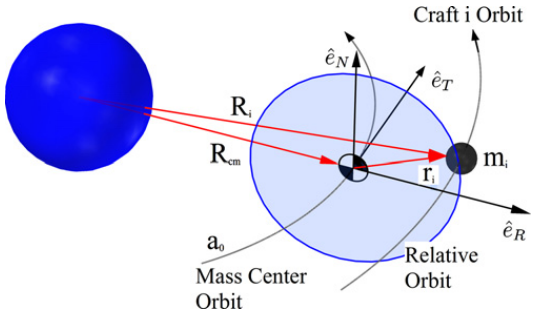

Fig. 1. Rotating hill-frame showing relative position vector $\mathbf{r}_i$.

CM is at the origin, the other craft's motion is determined explicitly from Eq. (5b)

$$\mathbf{G_1} = \begin{bmatrix} 2\omega\dot{y}_1 + 3\omega^2 x_1 \\ -2\omega\dot{x}_1 \\ -\omega^2 z_1 \end{bmatrix} \tag{5a}$$

$$0 = m_1\mathbf{r_1} + m_2\mathbf{r_2} \tag{5b}$$

where ω is the nominal CM orbit rate (or Hill-frame rotational rate with respect to inertial), and $L = r_{12}$ is the separation distance of the two craft. It is clear from Eq. (5b) that $\mathbf{r}_1$ and $\mathbf{r}_2$ are dependent, and in fact may be related via L using some mass fractions, as follows:

$$L = \|\mathbf{r_1} - \mathbf{r_2}\| = r_1/M_{r1} = r_2/M_{r2}$$
$$M_{r1} = \frac{m_2}{M_{\text{tot}}} = \frac{m_2}{m_1+m_2}, \quad M_{r2} = \frac{m_1}{M_{\text{tot}}} = \frac{m_1}{m_1+m_2} \tag{6}$$

The total craft 1 acceleration $\ddot{\mathbf{r}}_1$ is given by Eq. (7a), which results from substituting Eq. (5a) into Eq. (3), and using Eq. (5b) to eliminate the craft 2 state variables. The acceleration $\ddot{\mathbf{r}}_1$ is then a function of its own state-vector $\mathbf{X}_1$ only, and a potential-product $\Phi_{12} = \phi_1\phi_2$

$$\ddot{\mathbf{r}}_1 = \frac{\left(1+\frac{r_1}{M_{r1}\lambda_d}\right)}{\exp\left(\frac{r_1}{M_{r1}\lambda_d}\right)} \begin{bmatrix} \frac{\kappa_1\Phi_{12}x_1}{r_1^3} \\ \frac{\kappa_1\Phi_{12}y_1}{r_1^3} \\ \frac{\kappa_1\Phi_{12}z_1}{r_1^3} \end{bmatrix} + \begin{bmatrix} 2\omega\dot{y}_1 + 3\omega^2 x_1 \\ -2\omega\dot{x}_1 \\ -\omega^2\, z_1 \end{bmatrix} + \mathbf{u}_1 \tag{7a}$$

$$\kappa_1 = \frac{R_{sc}^2 M_{r1}^2}{k_c m_1}, \quad \mathbf{X}_1 = \begin{bmatrix} \mathbf{r}_1 \\ \mathbf{v}_1 \end{bmatrix} = \begin{bmatrix} x_1 \\ y_1 \\ z_1 \\ v_{x1} \\ v_{y1} \\ v_{z1} \end{bmatrix} \tag{7b}$$

2.3. Two-craft Coulomb formation equilibrium configurations and stability

Eqs. (5b) and (7a) admit three known static equilibrium configurations: Radial and Orbit-Normal as depicted in Fig. 2(a) and (b), and a third equilibrium (not shown) denoted Along-Track (the two craft are along the $\hat{e}_T$ line). A derivation of the conditions for equilibrium, summarized in Table 1, is given by Berryman and Schaub [5]. The constant Φ_{12} to achieve equilibrium, denoted Φ_{ref}, is dependent on m_1, m_2, and L. An attractive force is required for the Radial configuration, whereas the Orbit-Normal configuration requires a repulsive force.

The first order ODE systems are linearized about each equilibria, as defined by Eq. (4), yielding Jacobian matrices **A**. The linearized stability properties are determined from the eigenvalues of each **A**, and some of the important properties are summarized as follows [10,20]:

1. All three equilibrium configurations are dynamically unstable and the stability properties remain constant (i.e. there are no bifurcations, despite the eigenvalues dependence on: λ_d, m_1, m_2, and ω).
2. *Radial*: All eigenvalues are distinct. One is unstable and the other is stable, and both are real ($N_u = N_s = 1$). The stable/unstable eigenvectors are in the x–y plane. The center eigenspace (N_c=4) has one mode in the x–y plane and the other along the z-axis.
3. *Orbit-normal*: All eigenvalues are distinct. One unstable and one stable complex conjugate pair ($N_u = N_s = 2$), resulting in oscillatory modes with components in the x,

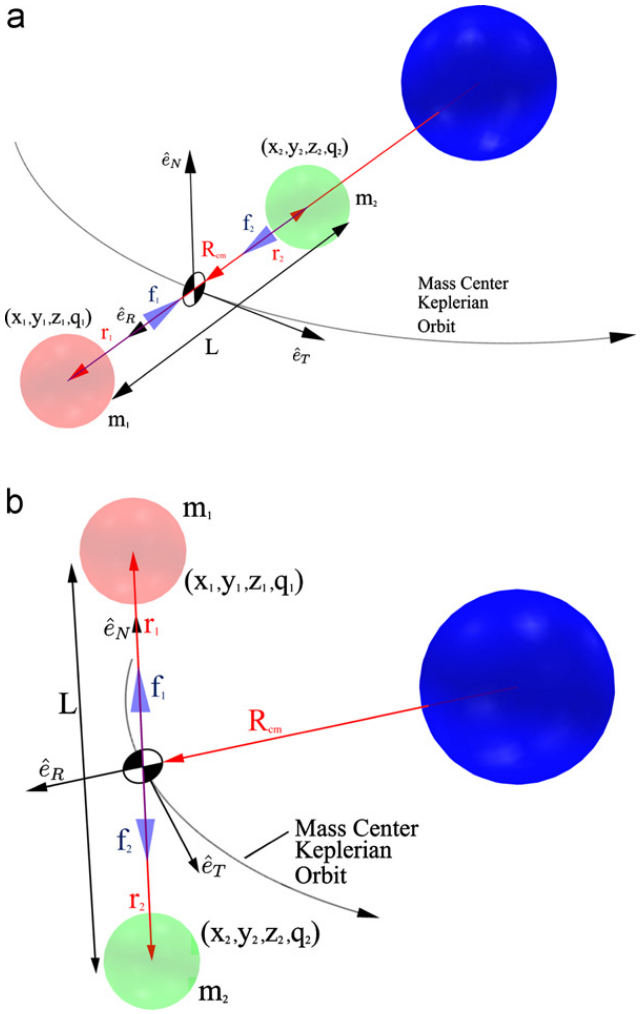

Fig. 2. Two-craft Coulomb formation equilibrium configurations in the hill-frame: (a) radial and (b) orbit-normal.

Table 1
Two-craft Coulomb formation equilibrium conditions.

Configuration	Craft 1 position, $\mathbf{r}_1$	Potential product Φ_{ref} (V^2)
Radial	$x_1 = M_{r1}L$ $y_1 = z_1 = 0$	$\frac{-3\omega^2 k_c m_1 m_2 L^3 e^{(L/\lambda_d)}}{R_{sc}^2\, M_{\text{tot}}(1+L/\lambda_d)}$
Orbit-normal	$x_1 = y_1 = 0$ $z_1 = M_{r1}L$	$\frac{\omega^2 k_c m_1 m_2 L^3 e^{(L/\lambda_d)}}{R_{sc}^2 M_{\text{tot}}(1+L/\lambda_d)}$
Along-track	$x_1 = z_1 = 0$ $y_1 = M_{r1}L$	0

y, and z directions. The center mode is along the z-axis ($N_c=2$).
4. *Along-track*: All eigenvalues associated with this configuration have zero real part ($N_c=6$), but there is a zero modulus repeated eigenvalue with algebraic multiplicity less than geometric multiplicity, making it unstable (albeit weakly).

3. Invariant manifold theory applied to Coulomb formations

The global stable and unstable manifolds (if they exist) are subspaces containing all trajectories (or flows) governed by the original nonlinear system dynamics ($\mathbf{F}$), with the following properties:

1. Unstable manifold (W^u): set of all trajectories which depart $\mathbf{X}^*$ asymptotically as $t\to\infty$.
2. Stable manifold (W^s): set of all trajectories which approach $\mathbf{X}^*$ asymptotically as $t\to-\infty$.
3. The manifolds are invariant, and therefore a state contained within W^u or W^s remains in that subspace for all time (e.g. $W^u\leftrightarrow W^s$ flows cannot occur).
4. The manifolds are tangent to their respective eigenspaces, in both $\pm$ directions at $\mathbf{X}^*$, and the $\pm$ yields two branches for W^u and W^s. Also, the manifold subspaces are 1-D higher than their corresponding eigenspaces (i.e. W^u has dimension of N_u+1).

The manifolds are created by initiating a small maneuver ($\Delta\mathbf{v}^{u/s}=\pm\epsilon E_{\mathbf{v}}^{u/s}$), where $E_{\mathbf{v}}^{u/s}$ indicates the velocity components of the normalized eigenvectors which span either E^u or E^s. When constructing W^u, the perturbed states $\mathbf{X}^{\mathbf{u}}=\mathbf{X}^*\pm\epsilon E_{\mathbf{v}}^u$ are propagated forward in time using $\mathbf{F}$ (from $t=0\to t_{\max}^u$), whereas for W^s the perturbed states $\mathbf{X}^{\mathbf{s}}=\mathbf{X}^*\pm\epsilon E_{\mathbf{v}}^s$ are propagated backward in time (from $t=0\to -t_{\max}^s$).

4. Generalized methodology for targeting optimal Coulomb reconfigurations along manifolds

Uncontrolled flows along manifolds, that complete as much of the transfer as possible, are sought first and provide a discontinuous initial guess (IG) trajectory to maneuver from some charged configuration to another. Control is then introduced to a portion of the IG, to differentially correct the flows to match continuity, while minimizing a scalar cost function J (e.g. total ΔV). The optimization problem is solved directly, by approximating the control functions $\phi_i(t)$ and $\mathbf{u}_i(t)$ (for each i craft), using a finite number of parameters. The general procedure for formulating and solving optimal Coulomb reconfigurations is outlined as follows:

1. Globalize the starting configuration unstable manifold ($\mathbf{X}^{\mathbf{u}}\subset W^u$) and target configuration stable manifold ($\mathbf{X}^s\subset W^s$). Then let $\mathbf{X}_i^{\mathbf{u}}\in W^u$ and $\mathbf{X}_i^s\in W^s$ denote particular manifold state vectors at the times $t_i^{u/s}$, where t_i^u and t_i^s denote propagation times along the respective manifold branches.
2. Define $\vec{\Psi}_i\subset(\mathbf{X}_i^{\mathbf{s}}-\mathbf{X}_i^{\mathbf{u}})$ to be a manifold state discontinuity vector, which must be driven to zero for a continuous trajectory. Next, t_i^u and t_i^s are found that minimize a scalar weighted norm function of $\vec{\Psi}_i$ (denoted ψ_i), within the bounds of Eq. (8). This yields quality propagation times: $t_{tot}^u\in\{t_{\min}^u,t_1^u,\ldots,t_{\max}^u\}$ and $t_{\text{tot}}^s\in\{t_{\min}^s,t_1^s,\ldots,t_{\max}^s\}$
$$t_{\min}^u\le t_{\text{tot}}^u\le t_{\max}^u,\quad t_{\min}^s\le t_{\text{tot}}^s\le t_{\max}^s \tag{8}$$
An IG transfer is thus established, with a state discontinuity function $\vec{\Psi}$ at the patch point time t_f, and total duration bounded below by $(t_{\min}^u+t_{\min}^s)$ and above by $(t_{\max}^u+t_{\max}^s)$. This trajectory is on W^u for $t:0\to(t_{\text{tot}}^u=t_f)$, and on W^s for $t:t_f\to(t_{\text{tot}}^s+t_f)$.
3. A number of control segments M (for each branch) and corresponding start times (τ_j^u and τ_j^s) are introduced, subject to Eq. (9), where M, $\tau_j^{u/s}$, and Eq. (8) bounds are inputs
$$0<\tau_{j-1}^u<\tau_j^u<t_f,\quad t_f<\tau_{j-1}^s<\tau_j^s<(t_f+t_{\text{tot}}^s)\ \ \forall j\in\{2\ldots M\} \tag{9}$$
4. A vector of independent decision variables $\mathbf{X_p}$ is defined, along with upper/lower limits on each element, where the elements consist of combinations of:
   - Impulsive changes to each $\mathbf{X}_i$ (e.g. $\Delta\mathbf{v}$).
   - The parameters used to approximate each $\phi_i(t)$ and $\mathbf{u}_i(t)$ piecewise, over each segment.
   - Segment start times (τ_j^u and τ_j^s) and manifold propagation times (t_{tot}^u and t_{tot}^s).

   A nonlinear programming solver is used to iterate on $\mathbf{X_p}$, to minimize some J, subject to $\vec{\Psi}=0$ (and any
5. inequality constraints).

In addition to using invariant manifolds in this optimal reconfiguration procedure, Jones [17] discusses some other potential applications of the theory, for Coulomb formation navigation and control purposes.

4.1. Charge control bounds for two-craft transfers

For the two-craft model presented in Sections 2.2–2.3, some bounding functions on parameterized $\phi_i(t)$ are derived by making the following assumptions:

1. The two potentials are equal in magnitude for all time $|\phi_1(t)|=|\phi_2(t)|$, and initially $\phi_1>0$. This then implies that if $\Phi_{ref}<0$ then $\Phi_{12}(t)=-\phi_1(t)|\phi_1(t)|$, otherwise $\Phi_{12}(t)=\phi_1(t)|\phi_1(t)|$.
2. The $\phi_1(t)$ control is approximated as either piecewise linear $\phi_1(t)=\phi_1(\tau_j)+\dot{\phi}_j(t-\tau_j)$ or impulsive $\phi_1(t)=\phi_1(\tau_j)+\Delta\phi_j$.
3. The patch point time t_f and segment start times $\tau_j^{u/s}$ remain fixed (and $\tau_j^{u/s}$ are equally spaced).

With these assumptions, ϕ_1 is denoted ϕ (ϕ_2 and Φ_{12} are computed explicitly), and $\phi^u(t)$ and $\phi^s(t)$ are used to denote ϕ_1 on each branch ($\phi_{\text{ref}}^{u/s}>0$). Enforcing $\phi(t_f)$ continuity provides the establishment of a lower bound on the parameters, as given by Eqs. (10a), (11a) for the impulsive model

and Eqs. (10b), (11b) for the linear model. These expressions ensure that $\phi^u(t_f)$ is capable of equaling $\phi^s(t_f)$; however, the problem will not always be constrained to have $\phi(t_f)$ continuity. Relaxing this continuity is reasonable so long as the jump from $\phi^u(t_f)$ to $\phi^s(t_f)$ can occur in a relatively short time. In the absence of power limits, this is generally valid since ϕ can be throttled very quickly [2].

- Case 1: $\Phi^u_{\text{ref}} \cdot \Phi^s_{\text{ref}} > 0$

$$|\Delta\phi^{u/s}|_{\text{bnd}} \geq |\phi^s_{\text{ref}} - \phi^u_{\text{ref}}| \tag{10a}$$

$$|\dot{\phi}^s|_{\text{bnd}} \geq \frac{|\phi^s_{\text{ref}} - \phi^u_{\text{ref}}|}{\tau^s_1 - t_f}, \quad |\dot{\phi}^u|_{\text{bnd}} \geq \frac{|\phi^s_{\text{ref}} - \phi^u_{\text{ref}}|}{t_f - \tau^u_1} \tag{10b}$$

- Case 2: $\Phi^u_{\text{ref}} \cdot \Phi^s_{\text{ref}} \leq 0$

$$|\Delta\phi^{u/s}|_{\text{bnd}} \geq \phi^s_{\text{ref}} + \phi^u_{\text{ref}} \tag{11a}$$

$$|\dot{\phi}^s|_{\text{bnd}} \geq \frac{|\phi^s_{\text{ref}} + \phi^u_{\text{ref}}|}{\tau^s_1 - t_f}, \quad |\dot{\phi}^u|_{\text{bnd}} \geq \frac{|\phi^s_{\text{ref}} + \phi^u_{\text{ref}}|}{t_f - \tau^u_1} \tag{11b}$$

Other requirements include $|I_{\text{out}}| > |I_{en}|$, and possibly a maximum power $P_{\text{out}} \leq P_{\max}$. Expressions for the maximum possible P_{out} as a function of: I_{out} and parameter bounds, are given by Eqs. (12a)–(12b), for the impulsive and linear models, respectively.

$$P_{\text{out}} = I_{\text{out}} \max\{|\phi^{u/s}_{\text{ref}}| + M|\Delta\phi^{u/s}|_{\max}\} \tag{12a}$$

$$P_{\text{out}} = I_{en} \max\{|\phi^{u/s}_{\text{ref}}| + |t_f - \tau^{u/s}_1||\dot{\phi}^{u/s}|_{\max}\} \tag{12b}$$

Lastly, an instantaneous ϕ change is only reasonable if steady-state is reached on a time-scale much less than the spacecraft dynamical response. An expression for ensuring impulsive model accuracy, is then given by Eq. (13), where $(\Delta t_q)_{\max}$ is the maximum allowable $\Delta\phi$ transition time. Eq. (13) can also be used in post-processing to determine solution validity, when not enforcing $\phi(t_f)$ continuity.

$$|\Delta\phi^{u/s}|_{\max} \leq \frac{k_c(\Delta t_q)_{\max} I_{\text{out}}}{R_{sc}} \tag{13}$$

Numerical values for the parameter bounds, and maximum required P_{out} and I_{out}, are computed based on the following two cases:

1. *Continuity of $\phi(t_f)$ is enforced.* For the impulsive model, $|\Delta\phi^u|_{\max}$ and $|\Delta\phi^s|_{\max}$ are set equal to the bounds given by Eq. (10a) or Eq. (11a), and I_{out} is increased from I_{en} until Eq. (13) is satisfied (P_{out} is computed from Eq. (12a)). For the linear model, the parameters are bounded using an input factor $0 \leq \gamma \leq 1$, according to Eq. (14), where $\phi_{\max}$ denotes the larger of $|\phi^s_{\text{ref}}|$ and $|\phi^u_{\text{ref}}|$. And, the maximum possible power is computed from Eq. (12b). For both models, a $P_{\max}$ requirement may be enforced by iterating on I_{out} and γ, respectively.

$$|\dot{\phi}^{u/s}|_{\max} = |\dot{\phi}^{u/s}|_{\text{bnd}} + \frac{\gamma\phi_{\max}}{|\tau^{u/s}_1 - t_f|} \tag{14}$$

2. *Continuity of $\phi(t_f)$ not enforced.* The parameter limits $|\Delta\phi^u|_{\max}$ and $|\Delta\phi^s|_{\max}$ (or $|\dot{\phi}^u|_{\max}$ and $|\dot{\phi}^s|_{\max}$), are inputs or computed from Eqs. (12a)–(12b) with a $P_{\max}$ requirement. For the impulsive case, Eq. (13) is solved for I_{out} using the larger $|\Delta\phi^{u/s}|_{\max}$.

5. Particle swarm optimization

The methodology of the previous section formulated the optimal Coulomb reconfigurations as nonlinear programming problems, whose methods of solution can be classified as either deterministic or stochastic. Deterministic or gradient methods require derivatives of J with respect to $\mathbf{X_p}$, and an initial guess (IG) for $\mathbf{X_p}$ that is within some unknown convergence tolerance, whereas stochastic methods generally require neither. In the paper by Jones [17], a variety of numerical difficulties encountered when applying a gradient solver to this methodology, are discussed. These obstacles (although not insurmountable), and the overall problem sensitivity, led to the adoption of a stochastic method. The stochastic method used here, is a variation of Particle Swarm Optimization (PSO), and it has thus far avoided many of the numerical and IG generation difficulties inherent in gradient methods.

PSO, introduced by Kennedy and Eberhart [18], is inspired by the motion of bird flocks searching for food. Pontani and Conway (among others) successfully apply PSO to optimal spacecraft trajectory problems including: impulsive and finite-burn transfers, low-thrust maneuvers, and targeting of Lyapunov orbit conditions in the CRTBP [19]. Moreover, PSO is often able to avoid local minima (unlike gradient methods) and in contrast to other stochastic methods it is very simple to implement. Its minor drawbacks include occasional difficulty in handling/satisfying constraints and an increase in computational complexity (relative to gradient methods) [19]. Specified bounds on the elements of $\mathbf{X_p}$ are required by PSO, but these may be justified using simple analytical expressions (as demonstrated in Section 4.1). The PSO implementation utilized in this work, closely follows that of Pontani and Conway [19], summarized as follows:

1. *Generate initial random population.* A population of M_{pop} individuals is created, each with a corresponding parameter vector $\mathbf{X_p}$ and an update/direction vector $\boldsymbol{\delta}\mathbf{X_p}$. The $\mathbf{X_p}$ components are uniformly and randomly generated within specified upper and lower bounds, and the $\boldsymbol{\delta}\mathbf{X_p}$ components (with bounds) are generated similarly.
2. *Begin iteration, at $l_0 = 1$.*
3. *Augmented performance index $\tilde{J}$ is computed for each individual at iterate l.* The performance index J is augmented with penalty function terms to account for and handle constraints. The equality constraints ($\vec{\Psi}_k = 0$) are treated according to Eq. (15a), where the weights α_k must be provided as inputs to the algorithm. Inequality constraints are handled differently as specified by Eq. (15b), where a very large $\tilde{J}$ is assigned if any inequality is violated, thereby enforcing feasibility

$$\tilde{J} = J + \sum_k \alpha_k |\vec{\Psi}_k| \tag{15a}$$

$$\text{Inequality violation}: \ \tilde{J} = \infty \quad \boldsymbol{\delta}\mathbf{X}_p(l) = 0 \tag{15b}$$

4. *Update $\mathbf{X_p}$ from $\boldsymbol{\delta}\mathbf{X_p}$ and enforce bounds.* The best parameter vector (yielding lowest $\tilde{J}$) for each i individual

(from $l_0 \ldots l$) is denoted as $\mathbf{Z}_p^i$. And the best parameter vector for the entire population (from $l_0 \ldots l$) is denoted as $\mathbf{Z}_{\min}$ (with global best cost $\tilde{J}_{\min}$). Each individual's direction and parameter vectors are updated according to Eqs. (16a)–(16c).

$$\boldsymbol{\delta}\mathbf{X}_\mathbf{p}(l+1) = C_I\boldsymbol{\delta}\mathbf{X}_\mathbf{p}(l) + C_C[\mathbf{Z}_\mathbf{p}(l) - \mathbf{X}_\mathbf{p}(l)] + C_S[\mathbf{Z}_{\min}(l) - \mathbf{X}_\mathbf{p}(l)] \tag{16a}$$

$$C_I = \frac{1+r_1}{2}, \quad C_C = 1.49445r_2, \quad C_S = 1.49445r_3 \tag{16b}$$

$$\mathbf{X}_\mathbf{p}(l+1) = \mathbf{X}_\mathbf{p}(l) + \boldsymbol{\delta}\mathbf{X}_\mathbf{p}(l+1) \tag{16c}$$

where the terms r_1, r_2, and r_3 are independent uniform random-numbers distributed over the interval (0,1), and computed at each l, and the terms C_I, C_C, C_S are inertial, cognitive, and social heuristics, respectively. After the update, each component of $\boldsymbol{\delta}\mathbf{X}_\mathbf{p}(l+1)$ is forced to be within its bounds. Furthermore, if any $\mathbf{X}_\mathbf{p}$ component violates its bound, that element is set to be on-boundary, and its corresponding $\boldsymbol{\delta}\mathbf{X}_\mathbf{p}$ component is set equal to zero.

Pontani and Conway use the heuristic functions of Eq. (16b) (optimized for various problems during early PSO performance research), and their procedure stops when a maximum number of iterations is reached [19]. In this work, Eq. (16b) heuristics are also adopted, but an alternate stopping criterion is proposed, where convergence is said to occur when: $\mathbf{Z}_{\min}$ satisfies all constraints to some tolerance (ϵ_1), and the average $\tilde{J}$ of the entire population is within a small tolerance (ϵ_2) of $\tilde{J}_{\min}$. The few variables that must be tuned when using this method are α_k, M_{pop}, and parameter bounds. The most problematic being the α_k values (penalty function weights), in that the PSO method has difficulty converging to a continuous transfer (i.e. satisfying $\vec{\Psi} = 0$) when the order of magnitude of any of these weights are set improperly.

6. Numerical test cases: optimal two-craft Coulomb formation reconfigurations

In this section, numerical demonstration cases are presented for Radial and Orbit-Normal reconfigurations.[1] For all numerical results, the two craft are assumed to have equal mass and radius R_{sc}, and Table 2 parameter values are used. These values closely follow those of Natarajan and Schaub [10], in their work on targeting such transfers. The mean value for λ_d at GEO is used [11], and the environmental current I_{en} is set at the worst-case value for GEO,[2] based on the previous research [2,23].

[1] The Along-Track is emitted due to the lack of unstable/stable modes in the linearized system.

[2] I_{en} is dependent on many factors including whether the vehicle is in sunlight or shadow and the magnitude of ϕ.

Table 2
Numerical test cases: input parameters.

Parameter	Value	Units
a_0	4.227×10^7	m
R_{sc}	1	m
λ_d	180	m
$m_1 = m_2$	150	kg
ω	7.2593×10^{-5}	rad/s
k_c	8.99×10^9	Nm^2/C^2
$\lvert I_{en} \rvert$	80	μA
$(\Delta t_q)_{\max}$	1	ms
ϵ	0.01	–
ϵ_1 **r**	$1.0e^{-3}$	m
ϵ_1 **v**	$1.0e^{-6}$	m/s
ϵ_2	$1.0e^{-7}$	–

6.1. Invariant manifold examples for the radial and orbit-normal configurations

Following the aforementioned procedure, global invariant manifolds associated with the Radial and Orbit-Normal configurations are generated, for $L = 25$ m, and integer values of the CM orbital period T_p for the propagation times. Although the system flows are parameter dependent (functions of λ_d, ω, m_1, and m_2), no bifurcations occur in the eigenspaces. Therefore, Figs. 3 and 4 (Radial) and 5(a), (b) (Orbit-Normal) are representative of the overall manifold structures. There is a substantial symmetry between stable and unstable branches (and the two vehicles, since $m_1 = m_2$).

The Radial configuration manifolds are planar and comparing Fig. 3 (stable) with Fig. 4 (unstable) suggests that nearly tangential crossings of the respective manifold branches are likely. Because of these observations, it is sensible to begin with transfers from one Radial configuration to another, which can be expansions (increase in L) or contractions (decrease in L). However, the Radial manifold + branches result in close encounters of the vehicles, and therefore targeting a practical transfer may require introducing a minimum allowable L constraint. The Orbit-Normal manifolds in Fig. 5(a) and (b) are seen to exhibit an oscillatory frequency in the x–y plane, and another along the z-axis (resulting in multiple crossings or piercings of the x–y plane).

6.2. Additional numerical reconfiguration assumptions

First, since two-craft formations are being considered, only the trajectories of craft 1 are plotted. This is because the CM condition of the Hill-frame model explicitly ensures the transfer of craft 2. Also, the reconfigurations along manifolds, once converged, are propagated forward in time to ensure that complete transfers are, in fact, achieved. A lengthly listing of the many permutations possible in the formulation of the optimal transfers, and their relevance is given by Jones [17]. In this

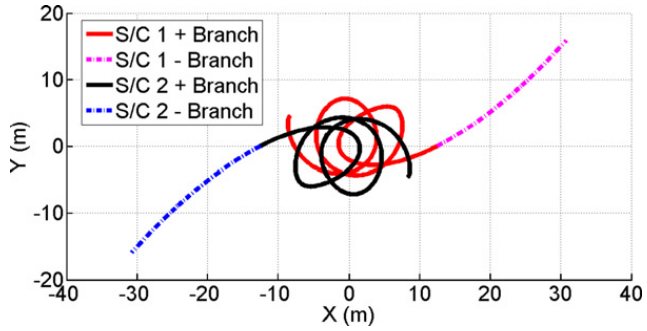

Fig. 3. Radial stable manifolds in hill-frame for spacecraft (S/C) 1 and 2: propagated $1T_p$.

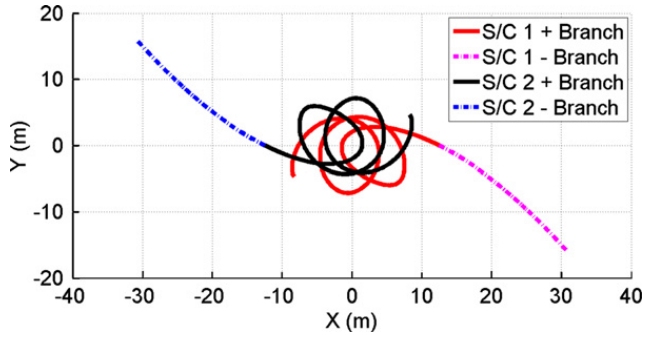

Fig. 4. Radial unstable manifolds in hill-frame for spacecraft (S/C) 1 and 2: propagated $1T_p$.

work, all results adhere to the following assumptions/limitations:

1. Only time-fixed optimal transfers are considered, with equally spaced control segments.
2. Coulomb thrusting is modeled as either impulsive or piecewise linear $\phi(t)$, and inertial thrusting is modeled as impulsive $\Delta\mathbf{v}_j$ maneuvers occurring at the $2M+1$ control segment nodes.
3. The performance index is $J=\Delta V=\sum_{j=1}^{M+1}\|\Delta\mathbf{v}_j\|$.

Also, Eq. (17a) is used to define ψ, a weighted norm function of $\vec{\Psi}$, and its minimal value yields: manifold propagation times (t^u_{tot} and t^s_{tot}) and IG trajectories

$$\psi_i=\sum_{k=1}^{3}|\mathbf{r}^s_{ki}-\mathbf{r}^u_{ki}|+\sum_{k=1}^{3}1000|\mathbf{v}^s_{ki}-\mathbf{v}^u_{ki}|$$
$$t^{u/s}_{\min}\le t^{u/s}_i\le t^{u/s}_{\max} \tag{17a}$$

where $\mathbf{r}^u_{ki}/\mathbf{r}^s_{ki}$ and $\mathbf{v}^u_{ki}/\mathbf{v}^s_{ki}$ denote unstable/stable position and velocity vector k components at: t^u_i/t^s_i.

6.3. Optimal radial expansion and contraction examples

As noted in Figs. 3 and 4, low-cost unstable to stable manifold transfers are easy to visualize (and converge upon) for the 2-D Radial configuration. Examples of a converged expansion ($L_0=25\rightarrow L_f=50$ m) and a contraction ($L_0=40\rightarrow L_f=15$ m) are demonstrated in Fig. 6(a) and (b). These optimized reconfigurations are generated with: $t^u_{\max}=t^s_{\max}=1.0T_p$ and $t^u_{\min}=t^s_{\min}=0.5T_p$ (total transfer bounded to around 1–2 days), and each k component of all

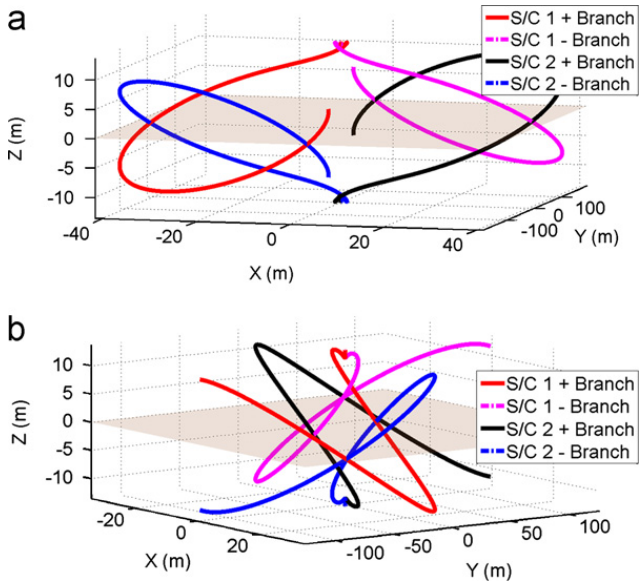

Fig. 5. Orbit-normal manifolds in hill-frame for spacecraft (S/C) 1 and 2: propagated $2T_p$: (a) stable and (b) unstable.

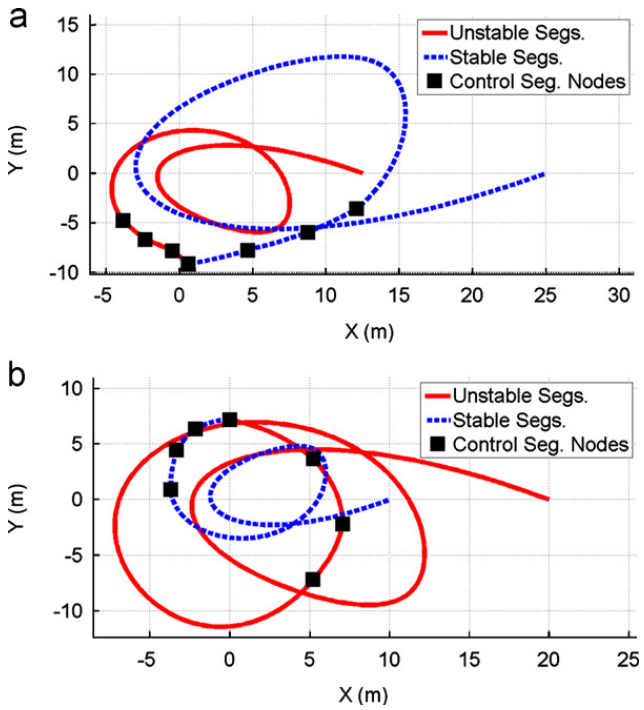

Fig. 6. Example optimal radial → radial reconfigurations: (a) expansion of: $L=25\rightarrow 50$ m and (b) contraction of: $L=40\rightarrow 20$ m.

$\Delta\mathbf{v}$ maneuvers bounded by: $\Delta v_k\le 1$ cm/s. Also, these radial reconfiguration examples have $M=3$, and $\tau^{u/s}_1$ set such that 85–87% of the total transfer durations are uncontrolled.

A linear ϕ parameterization with a ϕ discontinuity at t_f is used, and the maximum possible P_{out} are 4.4 W for the expansion (3.2 W for contraction). Optimal impulsive ϕ cases are also converged, for the same power bounds. The impulsive and linear ϕ expansions net optimal costs of $\Delta V=7.30$ mm/s and $\Delta V=6.76$ mm/s, respectively (transfer time of 1.54 days for both). The impulsive/linear ϕ contractions have $\Delta V=5.47$ mm/s/$\Delta V=6.22$ mm/s

(transfer time of 1.68 days for both). As further illustration, the $\phi(t)$ history and $\Delta\mathbf{v}$ radial ($\hat{e}_R$) and transverse ($\hat{e}_T$) component magnitudes are shown in Fig. 7(a) and (b), for the linear ϕ optimal solutions.

6.4. Radial expansions for varying problem formulations

This section demonstrates how the optimization problem formulation, and the values assigned to parameters in the methodology, affect the optimal solution. To qualitatively understand these changes, problem formulation parameters are altered, one at a time, from a nominal set of parameters. This is done for an expansion of $L_0 = 25 \rightarrow L_f = 30$ m, chosen because of the relative ease in obtaining converged solutions. An IG is targeted with total transfer bounded between 1 and 2 days, and 84% of the transfer uncontrolled ($\tau_1^u = 0.08 t_f$ and $\tau_1^s - t_f = 0.08 t_{\text{tot}}^s$), which yields the 1.03 day duration IG trajectory, shown in Fig. 8. Nominal optimal costs of $\Delta V = 3.01$ mm/s (impulsive) and $\Delta V = 2.75$ mm/s (linear) are found, for the following set of parameters: $M = 3$, $M_{\text{pop}} = 30$, $|\Delta\phi^{u/s}|_{\max} = 1$ kV, $|\dot{\phi}^{u/s}|_{\max} = 0.15$ V/s, $\Delta v_k \leq 1$ cm/s, and $\phi(t_f)$ continuity not enforced.

Tables 3 and 4 summarize changes to the optimal costs and iterations to converge, versus different problem formulation parameter values, for the impulsive model and linear model, respectively. The changes in cost are relatively small for all parameter variations, except for the $\phi(t_f)$ continuity assumption. This illustrates that good solutions are obtained with the nominal PSO setup.

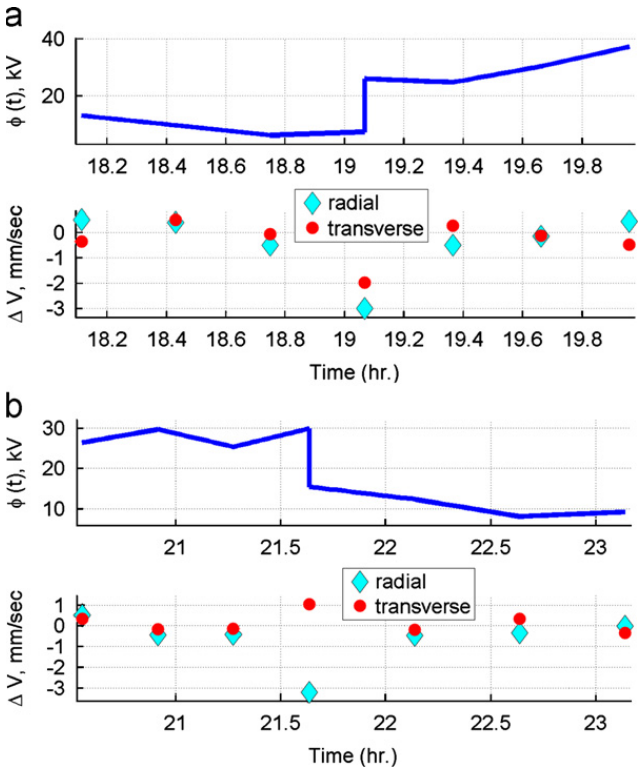

Fig. 7. Optimal control histories for radial → radial reconfiguration examples: (a) expansion of: $L = 25 \rightarrow 50$ m and (b) contraction of: $L = 40 \rightarrow 20$ m.

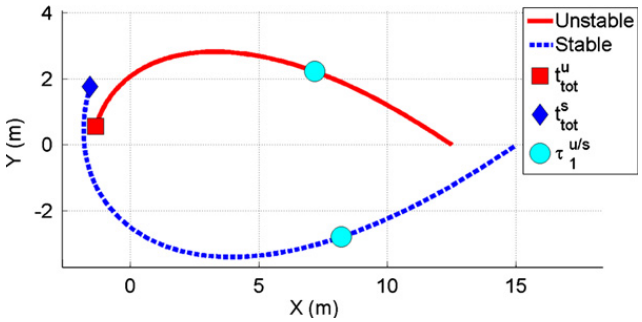

Fig. 8. Radial → radial expansion IG ($L = 25 \rightarrow 30$ m).

Table 3
Optimal radial expansion cost and iteration changes from nominal for: impulsive ϕ and $L = 25 \rightarrow 30$ m.

New parameter value	ΔV Change (mm/s)	Total iterate change
$M_{\text{pop}} = 20$	−0.5	−67
$M_{\text{pop}} = 60$	−0.032	−139
$\tau_1^u = 0.1 t_f$, $\tau_1^s - t_f = 0.1 t_{\text{tot}}^s$	−0.557	−23
$\tau_1^u = 0.2 t_f$, $\tau_1^s - t_f = 0.2 t_{\text{tot}}^s$	−0.931	+385
$\lvert\Delta\phi^{u/s}\rvert_{\max} = 2$ kV	+0.105	+44
$\lvert\Delta\phi^{u/s}\rvert_{\max} = 0.9$ kV	−0.270	−13
$\phi(t_f)$ continuous	+4.18	0

However, because the $\Delta\mathbf{v}$'s are being applied at the same times as $\phi(t)$ switching events, the manner in which the potentials are varied has a strong influence on the maneuver solution to connect the two manifolds. Changing the potential smoothly allows for practical considerations such as power usage to be included. But, the resulting optimal solutions are sensitive to how this smoothness is enforced.

In comparison, a $\phi(t)$ feedback controller (no inertial control) is used to expand and/or contract the Radial formation in the work of Natarajan [10,21]. The presented results using invariant manifolds are different in approach, specifically in having $\phi(t)$ held piece-wise constant. It is hypothesized that the resulting ΔV for expansions/contractions may be driven closer to zero for: increased M, higher order approximations for $\mathbf{u}(t)$ and $\phi(t)$, and further tuning of the PSO method. Moreover, while Natarajan employs linearizing assumptions to develop the reconfigurations, the presented method makes no small departure assumptions (beyond linearized gravity).

6.5. Optimal orbit-normal expansions and contractions

The manifolds associated with the Orbit-Normal configuration evolve more slowly, due to those modes having oscillatory parts, and therefore reconfigurations involving them will generally require more time. Similar to the Radial expansions, an Orbit-Normal expansion ($L_0 = 25 \rightarrow L_f = 50$ m) is provided as a numerical example, with a total transfer time bounded between 3 and 6 days. Fig. 9(a) and (b) illustrates the IG trajectory (with the

Table 4
Optimal radial expansion cost and iteration changes from nominal for: linear ϕ and $L=25\rightarrow30$ m.

New parameter value	ΔV increase (mm/s)	Total iterate change
$M_{pop}=20$	−0.245	−28
$M_{pop}=60$	+0.223	−100
$\tau_1^u=0.1t_f$, $\tau_1^s-t_f=0.1t_{tot}^s$	+0.249	+58
$\tau_1^u=0.2t_f$, $\tau_1^s-t_f=0.2t_{tot}^s$	+0.355	+74
$\lvert\dot{\phi}^{u/s}\rvert_{max}=0.3$ V/s	+0.318	+24
$\lvert\dot{\phi}^{u/s}\rvert_{max}=0.1$ V/s	+0.232	+25
$\phi(t_f)$ continuous	+2.43	+95

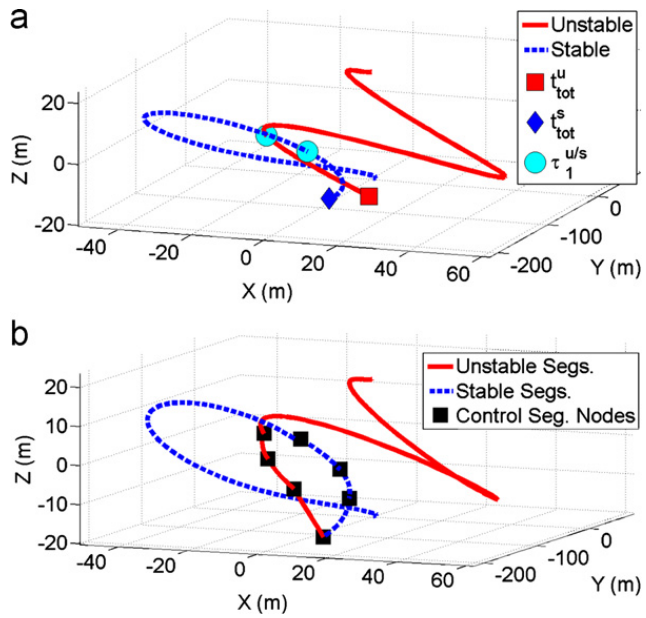

Fig. 9. Example orbit-normal → orbit-normal reconfiguration, Craft 1 → Craft 2, along manifolds: (a) IG expansion of: $L=30\rightarrow40$ m and (b) optimal expansion of: $L=30\rightarrow40$ m.

control start times $\tau_1^{u/s}$ shown), and a converged optimal solution, respectively. The reconfiguration is generated with: $\lvert\Delta\phi^{u/s}\rvert_{max}=2.0$ kV ($P_{out}<5.0$ W), $\Delta v_k\leq1$ cm/s, $M=3$, $M_{pop}=30$, $\tau_1^u=0.1t_f$, and $\tau_1^s-t_f=0.1t_{tot}^s$. Unlike in the transfers between Radial equilibria, this reconfiguration takes craft 1 from L_0 to the craft 2 slot with L_f (and craft 2→to craft 1). This provides ease of convergence by taking advantage of the anti-symmetry exhibited in the manifolds, and is reasonable, so long as: $m_1=m_2$ and for $\phi(t)$ not changing sign in the solution (crafts 1 and 2 are interchangeable). The transfer required $\Delta V=8.84$ mm/s, for a total duration of around 4.5 days.

6.6. Optimal orbit-normal to radial reconfigurations

The Orbit-Normal manifolds have multiple piercings of the x–y plane, with bounded x and z components. Whereas, the Radial manifolds are in the x–y plane, either near the origin or unbounded. Unfortunately for Orbit-Normal to Radial transfers, the x–y piercings occur at increasingly large y values, and the initial crossings occur such that the direction is opposite to that of any nearby opposing (stable or unstable) Radial manifold branches. Upon analysis, it can be concluded that the best use of invariant manifolds for such transfers is having only the Orbit-Normal branch controlled to target an unpropagated Radial state. Moreover, the best IG result from craft 1 to craft 2 transfers, and for Radial configurations with L slightly larger than the Orbit-Normal L.

An example Orbit-Normal → Radial expansion of this type ($L_0=15\rightarrow L_f=35$ m), is provided in Figs. 10(a)–(b). The IG in Fig. 10 shows vehicle 1 transferring to the Radial configuration craft 2 slot, which is stationary (unpropagated). The optimal impulsive ϕ solution is: $\Delta V=2.67$ mm/s (total transfer of around 1.65 days), for: $\lvert\Delta\phi^u\rvert_{max}=3$ kV ($P_{out}<5.2$ W), $\Delta v_k\leq1$ cm/s, $M=4$, $M_{pop}=30$, and $\tau_1^u=0.1t_f$. For this example, $\phi(t_f)$ continuity is not required; however, for realistic Orbit-Normal to Radial transfers this assumption would be a poor choice, since the $\phi(t_f)$ discontinuity is necessarily large. This is because Φ_{12} (and therefore ϕ) must change sign when transferring between these equilibria. Nevertheless, the example still demonstrates the best use of the invariant manifolds for this class of transfer.

7. Conclusions and future studies

Active charge control of closely flying spacecraft, result in Coulomb forces which supply a nearly propellant-less propulsion system, that avoids the problem of thruster impingement. These charged swarms admit numerous equilibrium configurations, that render 'virtual structures', referred to as so-called Coulomb formations. In the current work, a generalized method is developed for formulating and solving optimal transfers from one Coulomb configuration to another. The method exploits uncontrolled flow along invariant manifolds to complete

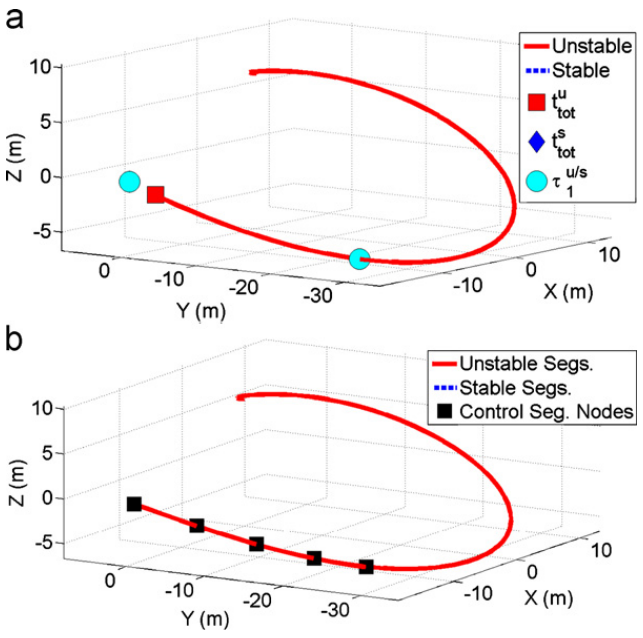

Fig. 10. Example orbit-normal → radial reconfiguration, Craft 1 → Craft 2, along unstable manifold: (a) IG expansion of: $L=15\rightarrow35$ m and (b) continuous expansion of: $L=15\rightarrow35$ m.

as much of the trajectory as possible, and therefore is useful for minimizing consumables; however, the natural motions necessitate transfers on the order of days. Invariant manifold theory is applied to two-craft Coulomb formations for the first time, and numerical results are presented, for these particular equilibria, demonstrating how optimal reconfigurations are targeted using this unique method.

A novel stochastic solver, Particle Swarm Optimization (PSO), inspired by the random motion of bird's seeking food, is successfully used to solve the parameter optimization problems. The PSO method eases many of the numerical and initial guess difficulties associated with these sensitive transfers; however, consistent PSO convergence remains challenging at times. Future work should attempt to address this, in part, by improving the numerical method, possibly by adopting a hybrid gradient/stochastic solver.

Further work will be directed in multiple directions. The first will be to apply invariant manifold theory to other known Coulomb formations (e.g. two-craft spinning and three-craft static), and analyze this motion to determine if reconfigurations may be targeted using the general method presented here. Second, inequality constraints that account for thruster plume impingement and minimum separation distance will be added to the optimization problem formulation. And finally the two-craft reconfigurations presented in this work will be explored in higher fidelity. This should include free segment start times, higher-order control approximations, and the inclusion of primary perturbations (i.e. solar radiation pressure) to ascertain their effect on the manifold structures and transfer trajectories.

Acknowledgments

The first author was supported by the Department of Defense's National Defense Science and Engineering Graduate Fellowship, which made this research possible.

References

[1] P. Lawson, J. Dooley, Technology Plan for the Terrestrial Planet Finder Interferometer, Technical Report 05-5, NASA Jet Propulsion Lab., 2005.
[2] L. King, C. Parker, S. Deshmukh, J. Chong, Spacecraft Formation-Flying Using Inter-Vehicle Coulomb Forces, Technical Report, NASA Institute for Advanced Concepts, 2002.
[3] L. King, C. Parker, S. Deshmukh, J. Chong, Study of interspacecraft coulomb forces and implications for formation flying, J. Propul. Power 19 (2003) 497–505.
[4] J.H. Cover, W. Knauer, H.A. Maurer, Lightweight Reflecting Structures Utilizing Electrostatic Inflation, US Patent 3,546,706, 1966.
[5] J. Berryman, H. Schaub, Analytical charge analysis for two- and three-craft coulomb formations, J. Guidance Control Dyn. 30 (2007) 1701–1710.
[6] E. Mullen, M. Gussenhoven, D. Hardy, Scatha, J. Geophys. Sci. 91 (1986) 1474–1490.
[7] E. Whipple, R. Olsen, Importance of differential charging for controlling both natural and induced vehicle potentials on ats-5 and ats-6, in: Proceedings of the Third Spacecraft Charging Technology Conference, 1980 pp. 888–893.
[8] C. Escoubet, M. Fehringer, M. Goldstein, The cluster mission, Ann. Geophys. 19 (2001) 1197–1200.
[9] H. Schaub, M. Kim, Orbit element difference constraints for coulomb satellite formations, in: AIAA/AAS Astrodynamics Specialists Conference, Paper No. 04-5213.
[10] A. Natarajan, H. Schaub, Hybrid control of orbit-normal and along-track two-craft coulomb tethers, in: AAS/AIAA Space Flight Mechanics Meeting, Paper No. 07-193.
[11] R. Inampudi, Two-craft Coulomb Formation Study About Circular Orbits and Libration Points, Ph.D. Thesis, University of Colorado, 2010.
[12] W. Clohessy, R. Wiltshire, Terminal guidance system for satellite rendezvous, J. Aerosp. Sci. 27 (1960) 653–658.
[13] E. Hogan, H. Schaub, Collinear invariant shapes for three-craft Coulomb formations, in: AIAA/AAS Astrodynamics Specialists Conference, Toronto, ON, Paper No. 2010-7954.
[14] H. Schaub, I.I. Hussein, Stability and reconfiguration analysis of a circularly spinning two-craft Coulomb tether, IEEE Trans. Aerosp. Electron. Syst. 46 (2010) 1675–1686.
[15] E. Hogan, H. Schaub, Linear stability and shape analysis of spinning three-craft coulomb formations, Celestial Mech. Dyn. Astron. 112 (2012) 131–148.
[16] R. Russell, T. Lam, Designing ephemeris capture trajectories at europa using unstable periodic orbits, J. Guidance Control Dyn. 30 (2007) 482–491.
[17] D. Jones, Optimal reconfiguration of coulomb formations along invariant manifolds, in: AAS/AIAA Spaceflight Mechanics Meeting, Paper No. 2012-104, Charleston, SC.
[18] J. Kennedy, R. Eberhart, Particle swarm optimization, in: Proceedings of the International Conference on Neural Networks, Piscataway, NJ, pp. 1942–1948.
[19] M. Pontani, B. Conway, Particle swarm optimization applied to space trajectories, J. Guidance Control Dyn. 33 (2010) 1429–1441.
[20] A. Natarajan, H. Schaub, Linear dynamics and stability analysis of a two-craft coulomb tether formation, J. Guidance Control Dyn. 29 (2006) 831–838.
[21] A. Natarajan, A Study of Dynamics and Stability of Two-Craft Coulomb Tether Formations, Ph.D. Thesis, Virginia Polytechnic Institute and State University, 2007.
[22] L. Stiles, C. Seubert, H. Schaub, Effective coulomb force modeling in a space environment, in: AAS/AIAA Spaceflight Mechanics Meeting, Paper No. 2012-105, Charleston, SC.
[23] L. Pettazzi, H. Kruger, S. Theil, D. Izzo, Electrostatic Forces for Satellite Swarm Navigation and Reconfiguration, Technical Report, European Space Agency, 2006.